ORIGINAL PAPER

Experiments on silicate melt immiscibility in the system Fe$_2$SiO$_4$–KAlSi$_3$O$_8$–SiO$_2$–CaO–MgO–TiO$_2$–P$_2$O$_5$ and implications for natural magmas

M. Bogaerts · M. W. Schmidt

Abstract The effect of CaO and MgO, with or without TiO$_2$ and P$_2$O$_5$, on the two-melt field in the simplified system Fe$_2$SiO$_4$–KAlSi$_3$O$_8$–SiO$_2$ has been experimentally determined at 1,050°–1,240°C, 400 MPa. Despite the suppressing effect of MgO, CaO, and pressure on silicate melt immiscibility, our experiments show that this process is still viable at mid-crustal pressures when small amounts (0.6–2.0 wt%) of P$_2$O$_5$ and TiO$_2$ are present. Our data stress that the major element partition coefficients between the two melts are highly correlated with the degree of polymerisation (nbo/t) of the SiO$_2$-rich melt, whatever temperature, pressure, or exact composition. Experimental immiscible melt compositions in natural systems at 0.1 MPa from the literature (lunar and tholeiitic basalts) plot on similar but distinct curves compared to the simplified system. These relations between melt polymerisation and partition coefficients, which hold for a large range of compositions and fO$_2$, are extended to various volcanic and plutonic rocks. This analysis strengthens the proposal that silicate melt immiscibility can be important in volcanic rocks of various compositions (from tholeiitic basalts to lamprophyres). However, the majority of proposed immiscible compositions in plutonic rocks are at least not coexisting melts, but may have suffered accumulation of early crystallized minerals.

M. Bogaerts (✉) · M. W. Schmidt
Institute for Mineralogy and Petrology, ETH-Zürich,
8092 Zürich, Switzerland
e-mail: michel.bogaerts@erdw.ethz.ch

Introduction

Silicate melt immiscibility has been proposed for many magmatic systems: mid-ocean ridge magma chambers (Dixon and Rutherford 1979), anorthosite complexes (e.g., Philpotts 1981), lunar and terrestrial volcanic rocks (Roedder and Weiblen 1971; Philpotts 1982), lamprophyre dykes (e.g., Philpotts 1976), granitoids (e.g., Kendrick and Edmond 1981; Rajesh 2003), and layered intrusions (McBirney 1975; Jakobsen et al. 2005). Occurrence of silicate melt immiscibility is actually difficult to assess from natural samples (e.g., Philpotts 1978; Biggar 1979), experimental data on immiscibility are thus necessary to clarify the role of melt immiscibility in nature. However, thorough studies have been limited to the system Fe$_2$SiO$_4$–KAlSi$_2$O$_6$–SiO$_2$ (Roedder 1951, 1978; Visser and Koster van Groos 1979a, b; Freestone and Powell 1983; Naslund 1983) at a pressure of 1,500 MPa, and to mid-ocean ridge and lunar basalts at 0.1 MPa (Rutherford et al. 1974; Hess et al. 1975; Dixon and Rutherford 1979; Ryerson and Hess 1980; Longhi 1990). A better understanding of the role played by important oxides in natural magmas (CaO and MgO) on silicate melt immiscibility is necessary to step from the system Fe$_2$SiO$_4$–KAlSi$_2$O$_6$–SiO$_2$ to natural magmas. The occurrence of stable silicate melt immiscibility depends on the relative positions of two surfaces: on one hand the two-melt surface of the miscibility gap and on the other hand the saturation surface of the liquidus minerals. CaO and MgO drastically suppress liquid immiscibility (Watson 1976a, b) by shrinking the two-melt field and also, for MgO, by increasing the liquidus temperature of Fe–Mg silicate minerals. While increasing pressure

widens the two-melt field, it also raises the liquidus of the crystalline phases and its overall effect is to reduce the stable two-melt field (Visser and Koster van Groos 1979b). On the contrary, TiO_2 and P_2O_5 expand the immiscibility field (Watson 1976a, b; Freestone 1978; Visser and Koster van Groos 1979c), counteracting the shrinkage of the stable two-melt field caused by addition of CaO or MgO and by increasing pressure. Previous experimental studies in simplified systems did not add the above groups of oxides (CaO–MgO and P_2O_5–TiO_2) concomitantly and therefore extrapolation to natural magmas at high pressures remained uncertain. In this study, we performed piston–cylinder experiments at 400 MPa and 1,050°–1,240°C in the system Fe_2SiO_4–$KAlSi_2O_6$–SiO_2, and then with progressive addition of CaO, MgO, P_2O_5, and TiO_2 to explore the effect of these components on the evolution of the two-melt field at a pressure representative for mid-crustal magma chambers. Our results, combined with literature data in the Fe_2SiO_4–$KAlSi_2O_6$–SiO_2 ± TiO_2 ± P_2O_5 ± CaO ± MgO show that the degree of melt polymerization is the key factor to discuss silicate melt immiscibility. Extending this finding to experiments on immiscibility in tholeiitic and lunar basalts gives an interesting tool to discuss immiscibility in natural magmas of various compositions.

Experimental procedure

Starting materials (Table 1) are mixtures of oxides (SiO_2, MgO, TiO_2), phosphates ($Ca_2P_2O_7$, $Mg_2P_2O_7$, K_3PO_4, $AlPO_4$), carbonate ($CaCO_3$), and silicate minerals (Fe_2SiO_4, $KAlSi_3O_8$). Oxides and carbonates were fired at 1,100°C for at least 4 h. All components were then mixed together in the desired proportions in an agate mortar and grinded for 40 min with ethanol. Products are then stored in a dessicator after drying for at least 1 day in an oven at 110°C. For each run, two starting materials were filled in a two-chamber Mo

capsule sealed in a Pt capsule. Experiments were mainly conducted in an end-loaded piston–cylinder with 14 mm bore and a NaCl–pyrex–graphite-crushable MgO assembly. Precision on the measured temperature is ± 5°C (Villiger et al. 2004). We applied a friction correction of –3% to the nominal pressure as has been obtained by calibration at 1.41 GPa and 1,000°C (Villiger et al. 2004), but a particular calibration at the low pressures investigated in this study (400 MPa) has not been performed. However, the systematics of the data suggest that the same pressure can be reproduced, even if it is not accurately known.

Mo capsules are ideal sample containers for several reasons. First, Fe loss to the capsule is low (Biggar 1970; Walker et al. 1972). Section analyses of the inner border of the Mo capsule show that Fe diffuses at a distance < 200 microns during 24 h at 1,150°C. Experiments producing only one melt show compositions close to the starting materials except for some minor Fe lost to the Mo capsule. Fe-loss increases with temperature: 6.8% at 1,150°C (Fx14, run B7), 8.8% at 1190°C (Fx15, run B19), and 11–12% at 1,240°C (Fx5c and Fx7c, run B21). Percentages are relative to total Fe, compare Tables 1 and 3. The contamination of silicate melts by the Mo-container is small, less than 0.21 and 0.05 wt% MoO_2 in the SiO_2-poor and SiO_2-rich melts, respectively. Mo is a high-field strength element and probably enhances the two-melt field. However, its low concentration suggests that its effect on the two-melt field is minor. Another advantage is the low oxygen fugacity imposed by the Mo-capsule. Walker et al. (1972) reported rim-crystallization of MoO_2 at 0.1 MPa, the fO_2 of their run being then on the Mo–MoO_2 buffer. Visser and Koster van Groos (1979a) calculated that this buffer is in the wüstite stability field, producing fO_2 slightly above the IW buffer at temperatures similar to this study. In our experiments, we crystallized a stoichiometric phase $FeMo_2O_5$, to our knowledge not described in the literature. The Fe-contaminated rim of the Mo capsule contains a maximum of 2 wt% Fe, which would expand

Table 1 Compositions (wt%) of the starting materials

	Fx5a	Fx5c	FX6	Fx7b	Fx7c	FX9	FX10	FX13	FX14	Fx15	FX20	Fx25	Fx26	Fx27
SiO_2	58.50	58.30	55.57	58.49	58.06	57.92	57.30	58.24	57.16	57.53	58.39	58.10	57.91	57.51
TiO_2	–	–	–	–	–	–	2.06	–	–	–	1.25	–	–	–
Al_2O_3	4.91	4.81	4.67	4.36	4.65	7.76	4.81	4.89	4.8	6.21	4.99	4.81	4.81	4.80
FeO_t	31.97	30.72	30.37	28.36	25.65	23.71	31.31	23.48	21.86	22.75	21.71	29.19	27.67	24.75
MgO	–	–	–	4.76	5.41	–	–	5.09	–	–	4.99	–	–	–
CaO	–	–	5.06	–	–	1.52	–	1.66	9.81	5.84	1.78	1.69	3.38	6.60
K_2O	4.54	4.50	4.31	4.03	4.29	7.17	4.45	4.52	4.43	5.74	4.61	4.48	4.47	4.45
P_2O_5	–	1.65	–	–	1.94	1.93	–	2.1	1.94	1.93	2.25	1.70	1.75	1.84

Fx5a is from Schmidt et al. (2006)

the stability field of Mo in T–fO_2 space by less than 0.1 log units, our fO_2 remaining below the Mo–MoO$_2$ buffer. Accordingly, almost all iron in our melts is Fe^{2+}.

Charges were mounted in epoxy, polished and then analyzed with the JEOL JXA-8200 at ETH-Zürich. Analytical conditions were set to an electron beam acceleration voltage of 15 kV, 10 nA beam current, and counting time of 20 s for all elements except of Ti and P (30 s). The beam diameter was 1 micron for mineral analyses and 5–10 microns for glass analyses.

Attainment of equilibrium

The phases obtained in our runs are melts (often a SiO$_2$-poor melt, L^M, coexisting with a SiO$_2$-rich melt, L^F), quartz, orthopyroxene, olivine, and ferrobustamite (a pyroxenoid). Minor phases are Mo–Fe oxides and a phosphate (withlockite or oxy-apatite) in some of the runs with CaO. Two main arguments exist to assess the equilibrium in our runs: (1) phases are homogeneous and do not show compositional variations within the

charge and (2) minerals contained in the different coexisting melts in the same charge have similar compositions (Fig. 1b).

Results

General

The compositions of the starting materials are given in Table 1, run conditions and results are summarized in Table 2, and analyses are presented in Table 3. All starting materials in experiments performed in the simplified system (this study; Watson 1976a, b; Visser and Koster van Groos 1979a, b, c and Freestone and Powell, 1983) have a ratio of Al/K = 1, as the relevant oxide components were added as feldspar component (orthoclase or gel). Both these elements enter preferentially into the SiO$_2$-rich melt, which shows, however, a greater affinity for K. This implies that the coexisting melts are not exactly in the Fe$_2$SiO$_4$–KAlSi$_3$O$_8$–SiO$_2$

Table 2 Experimental conditions and phase assemblage

Bulk	Run	T (°C)	Phases
System Fe$_2$SiO$_4$–KAlSi$_2$O$_6$–SiO$_2$ ± P$_2$O$_5$ ± TiO$_2$			
Fx5c	B18	1,130	LF, LM, Qtz
	B19	1,190	LF, LM
	B21	1,240	L
Fx10	B14	1,150	LF, LM, Qtz
System Fe$_2$SiO$_4$–KAlSi$_2$O$_6$–SiO$_2$–CaO ± P$_2$O$_5$			
Fx6	Z23	1,050	L, Fb, Ol, Qtz
Fx9	B6	1,150	LF, LM, Fa
Fx15	Z34	1,050	LF, LM, Pho
	B8	1,100	LF, LM
	B7	1,150	LF, LM
	B19	1,190	L
Fx14	Z34	1,050	LF, LM, Fb, Qtz, Pho
	B8	1,100	LF, LM, Qtz, Pho
	B7	1,150	L
Fx25	B24	1,150	LF, LM, Qtz
Fx26	B24	1,150	LF, LM, Qtz
	B25	1,190	L
Fx27	B26	1,150	LF, LM, Qtz
System Fe$_2$SiO$_4$–KAlSi$_2$O$_6$–SiO$_2$–MgO ± CaO ± P$_2$O$_5$ ± TiO$_2$			
Fx7b	B13	1,150	L, Px, Ol, Qtz
	B22	1,190	L, Px
Fx7c	B18	1,130	LF, LM, Px, Ol, Qtz
	B23	1,180	LF, LM, Px, Ol
	B16	1,150	LF, LM, Px, Ol
	B25	1,190	L
	B21	1,240	L
Fx13	Z32	1,150	LF, LM, Px, Ol
Fx20	B15	1,135	LF, LM, Px, Qtz
	B13	1,150	LF, LM, Px

Experimental pressure: 400 MPa. Running time: 24 h, except at 1,240°C (8 h)

L melt, *LF* SiO$_2$-rich melt, *LM* SiO$_2$-poor melt, *Px* orthopyroxene, *Ol* olivine, *Qtz* quartz, *Fb* ferrobustamite, *Fa* fayalite, *Pho* phosphate

Table 3 Electron microprobe analyses of experimental run products

Run	Bulk	T (°C)	Phase	n	SiO_2	TiO_2	Al_2O_3	FeO_t	MgO	CaO	K_2O	P_2O_5	Total
System Fe_2SiO_4–$KAlSi_2O_6$–SiO_2 ± P_2O_5 ± TiO_2													
B18	Fx5c	1130	LF	4	71.21	–	7.41	12.32	–	–	7.00	0.35	98.28
					0.76	–	*0.13*	*0.71*	–	–	*0.06*	*0.04*	
			LM	7	40.79	–	3.26	48.05	–	–	2.11	3.13	97.35
					0.91	–	*0.10*	*0.99*	–	–	*0.08*	*0.48*	
B19	Fx5c	1190	LF	4	67.92	–	5.95	17.86	–	–	5.90	0.73	98.35
					0.34	–	*0.03*	*0.36*	–	–	*0.04*	*0.03*	
			LM	4	47.14	–	3.72	42.25	–	–	2.95	2.78	98.84
					0.60	–	*0.10*	*0.64*	–	–	*0.07*	*0.12*	
B21	Fx5c	1240	L	6	59.15	–	4.92	27.30	–	–	4.37	1.34	97.08
					0.74	–	*0.11*	*1.00*	–	–	*0.08*	*0.07*	
B14	Fx10	1150	LF	3	66.71	1.23	6.22	17.95	–	–	6.18	–	98.27
					0.24	*0.02*	*0.10*	*0.27*	–	–	*0.02*	–	
			LM	4	45.44	3.34	3.45	43.51	–	–	2.31	–	98.06
					0.22	*0.04*	*0.02*	*0.33*	–	–	*0.37*	–	
System Fe_2SiO_4–$KAlSi_2O_6$–SiO_2–CaO ± P_2O_5													
Z23	Fx6	1050	L	3	60.61	–	6.05	20.19	–	5.15	5.55	–	97.54
					0.72	–	*0.15*	*0.85*	–	*0.21*	*0.25*	–	
			Ol	2	30.35	–	–	67.96	–	1.02	–	–	99.33
					0.33	–	–	*0.93*	–	*0.01*	–	–	
			Fb	2	47.77	–	0.37	35.73	–	15.65	–	–	99.51
					0.32	–	*0.04*	*0.14*	–	*0.07*	–	–	
B6	Fx9	1150	LF	3	69.26	–	9.54	9.49	–	0.53	9.29	0.61	98.73
					0.88	–	*0.29*	*0.44*	–	*0.05*	*0.25*	*0.36*	
			LM	3	32.65	–	2.23	51.44	–	3.94	1.85	5.74	97.86
					0.59	–	*0.12*	*0.36*	–	*0.18*	*0.17*	*3.19*	
Z34	Fx15	1050	LF	4	67.02	–	8.22	10.97	–	2.50	8.19	0.29	97.19
					0.74	–	*0.16*	*0.82*	–	*0.17*	*0.12*	*0.03*	
			LM	4	44.74	–	3.40	33.58	–	9.96	2.64	3.34	97.65
					0.30	–	*0.08*	*0.22*	–	*0.05*	*0.07*	*0.14*	
B8	Fx15	1100	LF	10	66.83	–	7.87	11.75	–	2.89	7.56	0.55	97.45
					0.38	–	*0.09*	*0.22*	–	*0.11*	*0.22*	*0.29*	
			LM	8	45.20	–	3.59	31.11	–	10.24	2.89	3.82	96.85
					0.74	–	*0.19*	*0.25*	–	*0.09*	*0.07*	*0.02*	
B7	Fx15	1150	LF	3	66.56	–	8.15	12.21	–	2.89	7.69	0.67	98.16
					0.46	–	*0.14*	*0.40*	–	*0.12*	*0.08*	*0.11*	
			LM	3	45.30	–	3.84	32.07	–	9.85	2.86	3.81	97.72
					0.65	–	*0.06*	*0.23*	–	*0.19*	*0.05*	*0.17*	
B19	Fx15	1190	L	4	57.75	–	6.24	20.73	–	5.12	5.58	1.77	97.19
					0.60	–	*0.05*	*0.34*	–	*0.09*	*0.09*	*0.08*	
Z34	Fx14	1050	LF	4	66.14	–	7.44	12.13	–	3.51	7.43	0.37	97.00
					0.08	–	*0.17*	*0.34*	–	*0.11*	*0.05*	*0.04*	
			LM	4	49.36	–	4.15	28.63	–	9.54	3.38	1.75	96.81
					0.23	–	*0.07*	*0.20*	–	*0.07*	*0.04*	*0.20*	
			Fb	3	47.50	–	0.30	32.01	–	19.12	–	–	99.05
					0.27	–	*0.16*	*0.66*	–	*0.64*	–	–	
B8	Fx14	1100	LF	4	65.10	–	6.19	13.48	–	5.46	6.57	0.51	97.31
					0.60	–	*0.11*	*0.43*	–	*0.21*	*0.12*	*0.11*	
			LM	2	55.56	–	4.45	21.69	–	9.96	4.27	1.24	97.19
					0.54	–	*0.21*	*0.57*	–	*0.30*	*0.19*	*0.05*	
B7	Fx14	1150	L	5	56.92	–	4.84	20.37	–	9.46	4.43	1.95	97.97
					0.50	–	*0.15*	*0.33*	–	*0.12*	*0.09*	*0.08*	
B24	Fx25	1150	LF	7	69.95	–	6.14	13.45	–	0.86	5.74	0.43	96.58
					1.24	–	*0.08*	*0.83*	–	*0.04*	*0.11*	*0.05*	
			LM	7	44.93	–	3.41	39.78	–	3.20	2.22	2.91	96.45
					0.78	–	*0.12*	*0.70*	–	*0.22*	*0.06*	*0.19*	

plane, the system being effectively quaternary (Freestone and Powell 1983). The Al/K ratios in our SiO_2-rich melts are 0.87–0.98 and 1.01–1.54 in the SiO_2-poor melts. These ranges are similar to those found by Watson (1976b) and Freestone and Powell (1983) who observed Al/K ratios between 0.86 and 1.06

Table 3 continued

Run	Bulk	T (°C)	Phase	n	SiO_2	TiO_2	Al_2O_3	FeO_t	MgO	CaO	K_2O	P_2O_5	Total
B24	Fx26	1150	LF	5	67.80	–	6.13	14.08	–	1.79	5.76	0.53	96.08
					0.89	–	0.10	0.34	–	0.07	0.08	0.06	
			LM	5	46.30	–	3.51	34.90	–	5.10	2.63	2.81	95.25
					0.89	–	0.10	0.43	–	0.10	0.11	0.20	
B26	Fx27	1150	LF	4	64.40	–	5.89	15.63	–	4.07	5.54	0.86	96.39
					0.57	–	0.05	0.35	–	0.12	0.05	0.04	
			LM	4	52.96	–	4.33	25.84	–	7.61	3.58	2.20	96.52
System Fe_2SiO_4–$KAlSi_2O_6$–SiO_2–MgO			$\pm$ CaO		$\pm$ P_2O_5	$\pm$ TiO_2								
B13	Fx7b	1150	L	3	73.95	–	8.34	6.50	0.35	–	7.72	–	96.86
					0.38	–	0.40	0.40	0.01	–	0.29	–	
			Px	2	49.98	–	0.25	38.39	11.93	–	–	–	100.55
					0.10	–	0.00	0.75	0.47	–	–	–	
			Ol	2	32.50	–	-	57.13	11.30	–	–	–	100.99
					0.34	–	-	2.40	1.85	–	–	–	
B22	Fx7b	1190	L	4	63.00	–	5.21	21.80	2.74	–	4.69	–	97.44
					0.67	–	0.10	0.93	0.18	–	0.18	–	
			Px	3	50.46	–	0.15	33.80	15.08	–	–	–	99.53
					0.69	–	0.04	0.25	0.39	–	–	–	
B18	Fx7c	1130	LF	5	72.02	–	7.19	8.36	0.76	–	7.38	0.65	96.36
					0.39	–	0.16	0.65	0.06	–	0.06	0.06	
			LM	4	37.83	–	2.79	40.93	4.84	–	2.35	7.47	96.21
					0.69	–	0.06	0.65	0.28	–	0.10	0.20	
			Px	4	49.87	–	0.19	34.48	14.25	–	–	–	98.85
					0.21	–	0.08	0.94	0.76	–	–	–	
			Ol	3	32.82	–	–	50.90	15.36	–	–	–	99.28
					0.14	–	–	0.18	0.40	–	–	–	
B23	Fx7c	1180	LF	6	68.39	–	6.73	12.66	1.50	–	6.52	0.96	96.75
					0.65	–	0.13	0.35	0.06	–	0.06	0.11	
			LM	5	42.87	–	3.44	37.44	4.35	–	2.92	5.51	96.52
					1.01	–	0.10	0.52	0.83	–	0.17	0.31	
			Px	12	50.32	–	0.19	33.63	15.16	–	–	–	99.35
					0.91	–	0.04	0.51	0.27	–	–	–	
			Ol	3	33.15	–	–	52.85	14.96	–	–	–	101.06
					0.12	–		0.20	0.23				
B16	Fx7c	1150	LF	5	71.68	–	7.35	9.63	0.96	–	7.03	0.68	97.32
					0.11	–	0.13	0.30	0.04	–	0.12	0.06	
			LM	9	38.21	–	2.96	40.54	4.37	–	2.42	7.18	95.67
					0.70	–	0.09	0.89	0.40	–	0.11	0.43	
			Px	7	50.40	–	0.18	33.79	15.09	–	–	–	99.52
					0.31	–	0.03	0.76	0.42	–	–	–	
			Ol	4	32.93	–	–	51.08	15.33	–	–	–	99.56
					0.48	–	–	0.36	0.77	–	–	–	
B21	Fx7c	1240	L	9	57.55	–	4.57	22.59	5.11	–	4.24	1.92	95.98
					0.76	–	0.12	0.40	0.18	–	0.13	0.12	
Z32	Fx13	1150	LF	4	72.44	–	8.49	6.92	0.41	0.59	8.43	0.44	97.71
					0.55	–	0.34	0.25	0.06	0.08	0.05	0.05	
			LM	4	29.33	–	2.54	37.56	3.37	7.40	1.80	13.38	95.38
					0.21	–	0.03	0.32	0.07	0.05	0.02	0.33	
			Px	5	48.63	–	0.22	39.18	10.41	0.85	–	–	99.34
					0.56	–	0.06	0.71	0.62	0.12	–	–	
B15	Fx20	1135	LF	9	72.29	0.75	7.27	7.67	1.03	0.71	7.11	0.51	97.34
					0.61	0.05	0.15	0.19	0.04	0.02	0.08	0.05	
			LM	8	39.41	2.34	2.87	32.13	5.11	4.72	2.19	7.08	95.85
					0.30	0.09	0.18	0.67	0.60	0.35	0.13	0.10	
			Px	4	50.89	–	0.15	31.61	15.67	0.68	–	–	99.24
					0.35	–	0.01	0.59	0.25	0.04	–	–	

in the SiO_2-rich melts and of 1.03–1.76 in the SiO_2-poor melts. Experiments performed by Visser and Koster van Groos (1979a, b, c) display a much wider and scattered range of values for Al/K due to significant K-loss during experiments: Al/K ranges between 0.59 and 1.79 in the SiO_2-rich melts and is 0.71–3.33 in the

Table 3 continued

Run	Bulk	T (°C)	Phase	n	SiO_2	TiO_2	Al_2O_3	FeO_t	MgO	CaO	K_2O	P_2O_5	Total
B13	Fx20	1150	LF	9	71.44	0.84	7.26	8.35	0.94	0.77	7.16	0.57	97.32
					_0.73_	_0.07_	_0.20_	_0.79_	_0.10_	_0.09_	_0.18_	_0.04_	
			LM	4	38.25	2.73	3.07	34.32	4.27	5.30	2.19	7.93	98.05
					_1.01_	_0.09_	_0.12_	_0.74_	_0.22_	_0.29_	_0.08_	_0.46_	
			Px	8	50.53	–	0.14	32.63	15.65	0.66	–	–	99.87
					_0.75_	–	_0.04_	_0.60_	_0.68_	_0.04_	–	–	

Number in italic are standard deviation (1 sigma)

_L_ melt, _LF_ SiO_2-rich melt, _LM_ SiO_2-poor melt, _Px_ orthopyroxene, _Ol_ olivine, _Fb_ ferrobustamite, _n_ number of analyses

SiO_2-poor melts. These K-losses should be kept in mind when observing discrepancies in P_2O_5 partitioning between the different data sets.

The system Fe_2SiO_4–$KAlSi_2O_6$–SiO_2 ±P_2O_5 ± TiO_2

Immiscible melts are easily analyzed by electronic microprobe; they quenched to homogeneous glasses and formed large bubbles and pools (Fig. 1a).

Hereafter, the SiO_2-rich melt will be termed felsic and properties are labeled with a superscript "F", the low-SiO_2 melt is termed mafic and labeled with a superscript "M". Two immiscibility fields exist in the system Fe_2SiO_4–$KAlSi_2O_6$–SiO_2 (Fig. 2a): a high-temperature field along the Fe_2SiO_4–SiO_2 join (above 1,695°C) and a low-temperature immiscibility field discovered by Roedder (1951). This latter immiscibility field has been well constrained by Roedder (1978), Visser and Koster van Groos (1979a) and Freestone and Powell (1983) at 0.1 MPa and by Visser and Koster van Groos (1979b) at higher pressures. It occurs along the fayalite–tridymite cotectic, separating a FeO-rich melt (corresponding to a simplified ferro-basalt) from a SiO_2-rich melt (ferro-dacitic in composition, Fig. 2a). At 0.1 MPa, the critical temperature of the miscibility gap is near 1,235°C, while the lowest temperature where two melts coexist is near 1,110°C. The high and low-temperature immiscibility fields are considered to be the stable parts of a common two-melt field partially below the cristobalite–trydimite liquidus (Visser and Koster van Groos 1979a).

Addition of P_2O_5

The two-melt field expands by adding P_2O_5 to a given composition in the Fe_2SiO_4–$KAlSi_2O_6$–SiO_2 system (Watson 1976a, b; Visser and Koster van Groos 1979c). Furthermore, the stability field of the silica mineral expands while the stability field of fayalite shrinks with increasing amounts of P_2O_5, as observed in other simplified systems (Kushiro 1975). Based on these observations, Ryerson and Hess (1980) proposed that phosphorus forms complexes by stripping metal cations from the silicate network and forcing the silica species to further polymerize. This causes an increase of the activity of SiO_2 and the destabilization of the "fayalite species" in the melt, increasing and reducing the stability field of the corresponding minerals, respectively. The expansion of the two-melt field is due to the lowering of the number of non-bridging oxygen (nbo) linked to the Si-tetrahedra, concomitant with the formation of P-complexes. The P-complexes cannot fit in a rigid silicate network, increasing the free energy of the system and the tendency to unmixing (Hess 1977). Accordingly, P_2O_5 is strongly enriched in the nbo-rich melt ($D_P^{M/F}$ between 3.8 and 8.9 in the system Fe_2SiO_4–$KAlSi_3O_8$–SiO_2–P_2O_5).

Experiments from this study and from Schmidt et al. (2006), without or with a small amount of CaO (Fx5a, Fx5c, Fx9), are projected from wollastonite and P_2O_5 into the Fe_2SiO_4–$KAlSi_3O_8$–SiO_2 plane (Fig. 2a). The orientation of the tie-lines, joining our coexisting melts, are similar to those of Visser and Koster van Groos (1979a, b, c). To illustrate the effect of P_2O_5 on the two-melt field, we consider a nearly isothermal section in the ternary diagram from Fe_2SiO_4 to a selected point on the $KAlSi_3O_8$–SiO_2 join. Compositions in this section are given by the KS/(Fe_2SiO_4 + KS) ratio, where KS is the composition along the $KAlSi_3O_8$(K)–SiO_2(S) join (Fig. 3). Data plotted in Fig. 3 are from similar bulk compositions in the Fe_2SiO_4–$KAlSi_3O_8$–SiO_2 system with variable P_2O_5 content: Fx5a (no P_2O_5; Schmidt et al. 2006), Fx5c (1.65 wt% P_2O_5; this study), F, and J (0.6 and 2.9 wt% P_2O_5, respectively; Visser and Koster van Groos 1979c). These experiments illustrate the expansion of the two-melt field by adding P_2O_5 to the composition Fx5a, as well as the importance of both the P_2O_5 content and the KS/ (Fe_2SiO_4 + KS) ratio to determine the length of the tie-lines. Without P_2O_5, all bulk compositions lying on a given tie-line in the system Fe_2SiO_4–$KAlSi_2O_6$–SiO_2

should give the same coexisting melts in different proportions. If the same amount of P_2O_5 is added to these bulk compositions, the length of the tie-lines will be longer for the most polymerized bulk composition. This explains why the bulk composition Fx9 produces more extreme coexisting melts than Fx5c, despite having similar P_2O_5 contents (1.9 and 1.6, respectively): the former starting material has a higher KS/(Fe_2SiO_4 + KS) ratio than the latter.

Addition of TiO$_2$

Immiscibility experiments in the system Fe_2SiO_4–KAlSi$_2$O$_6$–SiO$_2$–TiO$_2$ (Visser and Koster van Groos 1979c) and phase relationships in MgO–SiO$_2$–CaAl$_2$Si$_2$O$_8$ (Kushiro 1975) showed that adding TiO$_2$ to silicate melts has the same effect as P_2O_5, however with smaller amplitude. A solution mechanism similar to that proposed for P_2O_5 is also valid for TiO$_2$, but is certainly not the only one (Mysen et al. 1980; Ryerson 1985). Indeed, spectroscopic data demonstrate that Ti in silicate melts may have three coordination numbers: 4, 5, and 6-fold, with their relative abundances depending on melt composition (Farges and Brown 1997). [4]Ti and [5]Ti units may co-polymerize with the Si-tetrahedron or form complexes, while [6]Ti is a network modifier or complex former. The partitioning of Ti between these three entities (Si–Al network, complexes, and network modifiers) probably explains its reduced effect on immiscibility compared to P_2O_5, which only forms complexes (Hess 1991).

Our experiment with a starting material containing 2 wt% TiO$_2$ (Fx10) produces coexisting melts slightly more differentiated than those obtained at the same condition (1,150°C and 400 MPa) with a similar bulk composition in the system Fe_2SiO_4–KAlSi$_2$O$_6$–SiO$_2$ (Fx5a, Fig. 2a), in agreement with Visser and Koster van Groos (1979c). However, our data set does not allow us to quantitatively compare the effect of P_2O_5 and TiO$_2$.

Effect of CaO in the system Fe_2SiO_4–KAlSi$_2$O$_6$–SiO$_2$ ± P_2O_5

Hoover and Irvine (1978) performed experiments at 0.1 MPa with bulk compositions in the plane Fe_2SiO_4–CaSiO$_3$–K$_{56}$S$_{44}$ of the Fe_2SiO_4–KAlSi$_3$O$_8$–SiO$_2$–CaSiO$_3$ tetrahedron (Fig. 2b). This plane is of interest because it is close to the orthoclase–quartz–fayalite eutectic (K$_{59}$S$_{41}$) and because the Fe_2SiO_4–K$_{56}$S$_{44}$ join passes through the low-temperature immiscibility field of the pseudo-ternary Fe_2SiO_4–KAlSi$_2$O$_6$–SiO$_2$.
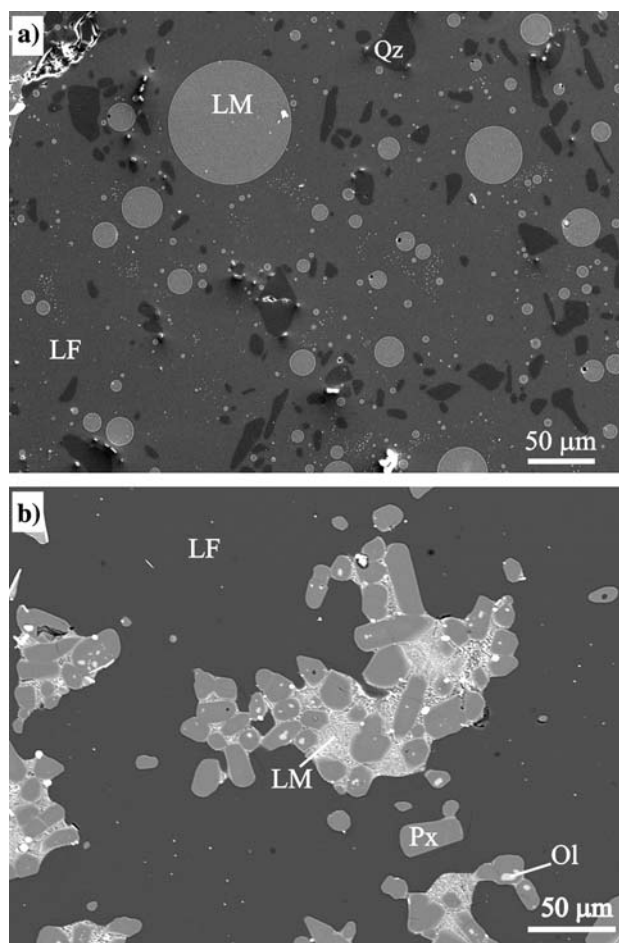
Fig. 1 Back-scattered electron images of experimental charges. **a** Experiment in the system Fe_2SiO_4–KAlSi$_3$O$_8$–SiO$_2$–P$_2$O$_5$ at 1,150°C and 400 MPa (experiment B18, starting material Fx5c). **b** Experiment in the system Fe_2SiO_4–KAlSi$_3$O$_8$–SiO$_2$–MgO–P$_2$O$_5$ at 1,180°C and 400 MPa (experiment B23, starting material Fx7c); olivine form small crystals usually included in pyroxenes. *Bright spots* are Mo sequestrated from the capsule walls by the melt. *LF* SiO$_2$-rich melt, *LM* SiO$_2$-poor melt, *Px* pyroxene, *Ol* olivine, *Qz* quartz

Fe-bearing silicate minerals crystallizing in the system Fe_2SiO_4–Hd'–K$_{56}$S$_{44}$ (Fig. 2b, Hd' is the projection of hedenbergite component onto the plane Fe_2SiO_4–CaSiO$_3$–KS) are fayalite and ferrobustamite. By adding a small amount of CaO, Hoover and Irvine (1978) observed that both the liquidus and the two-melt fields are depressed. The latter quickly becomes metastable but reappears along the fayalite–ferrobustamite cotectic curve in the middle of the Fe_2SiO_4–Hd'–K$_{56}$S$_{44}$ plane. The shape of the two-melt field along the fayalite–ferrobustamite cotectic is not well constrained, nevertheless, Hoover and Irvine (1978) observed that the critical temperature of the central miscibility gap lies no more than 10°C above the liquidus. If the upper limit of the immiscibility field is that close to the
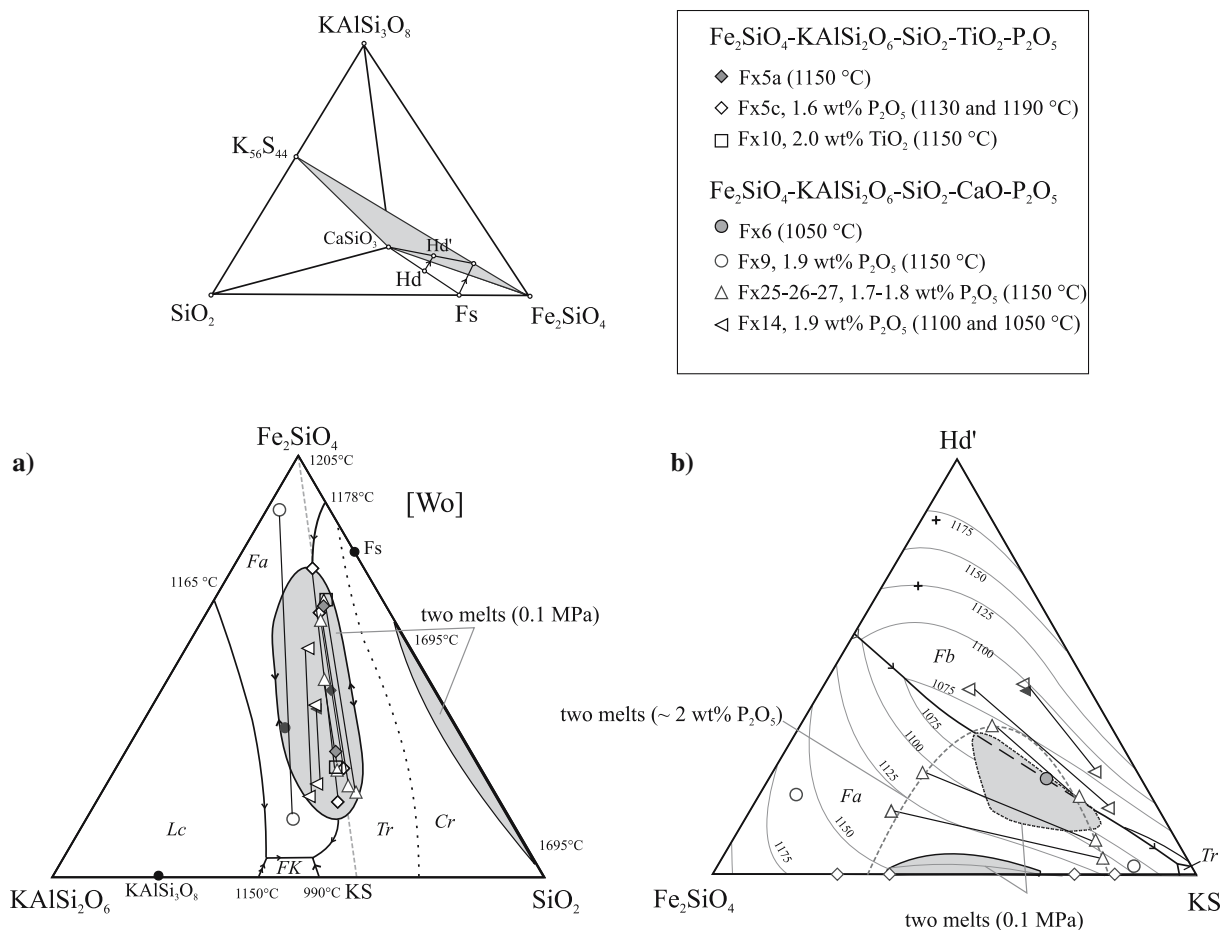
Fig. 2 Melt compositions in the KAlSi$_3$O$_8$–CaSiO$_3$–Fe$_2$SiO$_4$–SiO$_2$ tetrahedron (projected from TiO$_2$ and P$_2$O$_5$). **a** Projection from wollastonite [Wo] onto the plane Fe$_2$SiO$_4$–KAlSi$_3$O$_8$–SiO$_2$. The starting materials are represented by the *black symbols*: *diamond* (Fx5a and Fx5c), *triangle* (Fx14), *circle* (fx9). The starting materials of Fx25–Fx26–Fx27 are between Fx5c and Fx14 bulk compositions. Crystallization curves and immiscibility fields (*gray shaded areas*) at 0.1 MPa are after Roedder ([1951](#), [1978](#)), Visser and Koster van Groos ([1979a](#)). *Lc* leucite, *Fa* fayalite, *FK* K-feldspar, *Cr* cristobalite, *Tr* Tridymite, *Fs*

ferrosilite. **b** The plane Hd'–Fe$_2$SiO$_4$–K$_{56}$S$_{44}$ (56 wt% KAlSi$_3$O$_8$ and 44 wt% SiO$_2$) at 0.1 MPa from Hoover and Irvine ([1978](#)), depicted by the *gray shaded plane* in the tetrahedron. Hd' is the orthogonal projection (parallel to the KAlSi$_3$O$_8$–SiO$_2$ axis) of hedenbergite (Hd: CaFeSi$_2$O$_6$) from the plane Fe$_2$SiO$_4$–SiO$_2$–CaSiO$_3$ onto the plane Fe$_2$SiO$_4$–KS–CaSiO$_3$. The *gray shaded areas* are the two-melt fields at 0.1 MPa. The various symbols are data from this study. The *crosses* represent the projections of the ferrobustamite compositions [Z23 (Fx6) and Z34 (Fx14)]. Same abbreviations as 2a, except Fb (ferrobustamite)

liquidus, it is unlikely that the immiscibility field persists at significantly higher pressures. Indeed, in the Fe$_2$SiO$_4$–KAlSi$_2$O$_6$–SiO$_2$ system, in which the two-melt field rises 90°C above the liquidus at 0.1 MPa, Visser and Koster van Groos ([1979b](#)) observed that the miscibility gap becomes metastable near 650 MPa, as the liquidus temperatures of the silica mineral and fayalite increase with a steeper dP/dT slope than the critical temperature. One of our experiments in the Fe$_2$SiO$_4$–Hd'–KS plane at 400 MPa confirms the rapid suppression of the two-melt field by the temperature increase of the liquidus surface. At 1,050°C, the starting material Fx6 produces a melt (with K$_{56}$S$_{44}$) saturated with fayalite, ferrobustamite, and quartz. Clearly,

the presence of CaO in silicate melt greatly inhibits the two-melt field at mid-crustal pressure. However, the addition of approximately 2 wt% P$_2$O$_5$ to bulk compositions containing CaO (Fx25, Fx26, Fx27, Fx14, Fx15: Table [1](#)) and being close to the K$_{56}$S$_{44}$ plane (Fig. [2](#)a) produces extensive melt immiscibility at 1,170°–1,050°C and 400 MPa. The starting material with the highest CaO content (Fx14: 10 wt% CaO) produces two melts plus quartz at 1,100°C and two melts plus quartz and ferrobustamite at 1,050°C. A phosphate mineral is also present, forming small elongated crystals not large enough to analyze properly. Contaminated analyses make it difficult to distinguish between oxy-apatite, Ca$_{10}$(PO$_4$)$_6$O, or
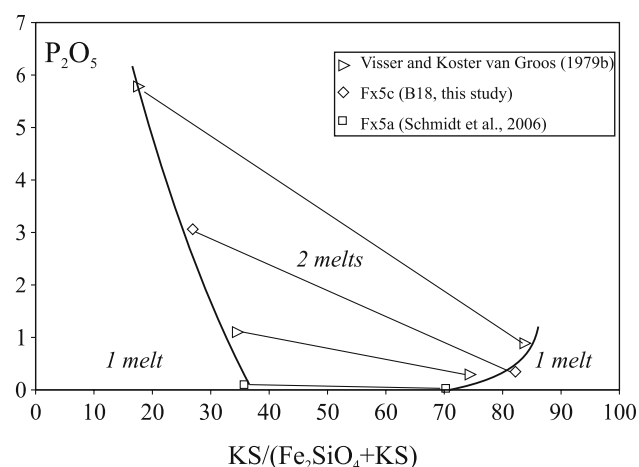
Fig. 3 Section of the Fe_2SiO_4–$KAlSi_2O_6$–SiO_2 plane along Fe_2SiO_4–$K_{49}S_{51}$ (49 wt% $KAlSi_3O_8$ and 51 wt% SiO_2) illustrating the effect of P_2O_5 and $KS/(Fe_2SiO_4 + KS)$ ratio of the bulk composition on the length of tie-lines between coexisting melts. Conditions of the experiments: Fx5a (no P_2O_5, 1,150°C, 400 MPa), Fx5c (1.65 wt% P_2O_5, 1,165°C, 400 MPa). Data from Visser and Koster van Groos (1979b): J (2.9 wt% P_2O_5, 1,165°C, 500 MPa), F (0.6 wt% P_2O_5, 1,150°C, 300 MPa)

whitlockite, $Ca_3(PO_4)_2$. The triangular symbols map the two-melt field in Fe_2SiO_4–Hd'–$K_{45–51}S_{55–49}$ at 1,150°C (dashed line in Fig. 2b) for bulk compositions with ~ 2 wt% P_2O_5 between Fx5c (no CaO) and Fx14 (10 wt% CaO), the latter resulting in only one melt at this temperature. These observations support the suggestion of Hoover and Irvine (1978; at 0.1 MPa) that their miscibility gaps are the stable, outcropping parts of the same two-melt field. Experiments on the bulk compositions Fx9 (1.52 wt% CaO and 1.93 wt% P_2O_5) and Fx15 (5.84 wt% CaO and 1.93 wt% P_2O_5, not plotted in Fig. 2 for clarity) produce longer tie-lines due to a higher $KS/(Fe_2SiO_4 + KS)$ ratio. Experiments with the Fx15 bulk compositions indicate that the two-melt field extends far above the liquidus: with the exception of a phosphate mineral at 1,050°–1,100°C, two melts appear without further coexisting minerals between 1,050 and 1,190°C. The enhancement of the two-melt field is due to the influence of P_2O_5 on the miscibility gap itself and to the depression of the silicate mineral liquidus.

Effect of MgO in the system Fe_2SiO_4–$KAlSi_2O_6$–$SiO_2 \pm P_2O_5$

To our knowledge, there are no experiments available inside the Mg_2SiO_4–Fe_2SiO_4–$KAlSi_3O_8$–SiO_2 tetrahedron. The Mg_2SiO_4–$KAlSi_3O_8$–SiO_2 and Mg_2SiO_4–Fe_2SiO_4–SiO_2 ternary systems have been studied by Luth (1967) and Bowen and Schairer (1935), respec-

tively. A brief description of the Mg_2SiO_4–Fe_2SiO_4–SiO_2 system follows (Fig. 4a) to help the discussion of our experiments in the Mg_2SiO_4–Fe_2SiO_4–KS plane (Fig. 4b). The isobaric (0.1 MPa) invariant point L at 1,305°C corresponds to the peritectic reaction: olivine + melt = pyroxene + trydimite. The cristobalite–trydimite field is bound by two univariant curves: melt-SiO_2 polymorph–pyroxene and melt-SiO_2 polymorph–olivine. As observed in other ternary systems (e.g., Mg_2SiO_4–$CaMgSi_2O_6$–SiO_2 and Fe_2SiO_4–$CaFeSi_2O_6$–SiO_2: Hoover and Irvine 1978), melts evolve toward low-SiO_2 compositions by crystallization. The addition of $KAlSi_3O_8$ drastically reduces the stability field of the silica mineral. This field is constrained in Fig. 4b by the intersection of the fayalite–trydimite and pyroxene–trydimite cotectic curves with the $(Mg,Fe)_2SiO_4$–KS joins at 0.1 MPa (Mg_2SiO_4–KS from Luth 1967 and Fe_2SiO_4–KS from Visser and Koster van Groos 1979a). This latter join intersects the low-temperature immiscibility field (Fig. 4b, c).

Replacing some FeO by a small amount of MgO (± 5 wt%: compare Fx5a and Fx7b in Table 1) increases the liquidus temperature and renders the two-melt field metastable. At 1,150°C the bulk composition with 5 wt% MgO (Fx7b) produced a high-silica melt (73.9 wt% SiO_2, run B13) coexisting with quartz, orthopyroxene, and olivine, while two melts without coexisting minerals occur in the Mg-free system at the same temperature (Fx5a). The assemblage melt-orthopyroxene–olivine–quartz corresponds to the point L in Fig. 4a. The melt plots very close to the Fe_2SiO_4–KS joint, implying that olivine + quartz only coexist with a melt having a very high FeO/MgO ratio. At 1,190°C, the same starting material gives a less differentiated melt (63.0 wt% SiO_2, run B22, open circle in Fig. 4b, c) in equilibrium with orthopyroxene. Along with the position of the pyroxene–olivine crystallization curve on the join Mg_2SiO_4–SiO_2 (Luth, 1967), the pyroxene stability field can be roughly drawn in the Mg_2SiO_4–Fe_2SiO_4–KS plane (Fig. 4b). The strong bending of the pyroxene–olivine crystallization curve is associated with the metastable immiscibility field and is also apparent in the system Fe_2SiO_4–$CaFeSi_2O_6$–SiO_2 saturated with a Ca-rich pyroxene (Hoover and Irvine 1978). The addition of ~ 2 wt% P_2O_5 to the starting material with 5 wt% MgO (Fx7c) renders the two-melt field stable; two melts coexist with abundant orthopyroxene, a small amount of olivine (Fig. 1b), and with additional quartz at low temperature (1,130°C). The silica-poor, phosphorus-rich melts suffered unmixing upon quench, especially in the small pools of mafic melts in the pyroxene aggregates (Fig. 1b). Analyses of these pools give more

extreme compositions (lower silica content) than the larger pools in the same aggregates or along the rim of the capsule. The analyses of these latter pools are homogeneous in a given charge and are thus considered to define the composition of the mafic melt. It is difficult to identify whether the slight increase in the length of the tie-lines compared to those in the system Fe_2SiO_2–$KAlSi_3O_8$–SiO_2 is due to MgO or to the higher P_2O_5 content in Fx7c (1.94 wt%) than Fx5c (1.65 wt%). Experiments with these two starting materials at 1,190°C yield contrasting assemblages: two melts coexist in the MgO-free system (Fx5c) while only one melt is present when MgO is added (Fx7c). The two-melt field plunges downward from the Fe_2SiO_4–SiO_2 side to the Mg_2SiO_4–SiO_2 side. In summary, MgO does not favor immiscibility, as it increases liquidus temperatures and lowers the critical temperature. This behavior is different from CaO which reduces both the liquidus temperature and the two-liquid field (Fig. 2a, c).

The addition of small amounts of CaO and TiO_2 (starting material Fx20) does not have an important effect on the width of the two-melt field. A noticeable difference is that olivine is no longer stable with the two melts and orthopyroxene. Compared to the system without CaO and TiO_2, both elements lower the liquidus temperature of olivine.

Discussion

Effect of melt structure on partition coefficients between immiscible melts

Fe, Mg and Ca partitioning

The influence of melt structure on trace and major element partitioning between silicate melt and minerals have been outlined by several experimental studies (e.g., Watson 1976a, b; Ryerson and Hess 1978; Kohn and Schofield 1994; Mysen 2004; Schmidt et al. 2006). The parameter nbo/t (nbo: number of non-bridging oxygens, t: tetrahedrally coordinated network former cations) is frequently used to express the degree of polymerization in silicate melts (Mysen 1983). For melts containing P and Ti, this parameter is difficult to calculate, as these cations may either polymerize the melt by partially substituting for Si (Ti) or by stripping metallic cations to form complexes (P and Ti). Ti can also act as a network modifier (e.g., Mysen 1990; Farges and Brown 1997). Both cations partition into the less polymerized, low-SiO_2 melt, demonstrating that Ti and P have a structural role different from that

of Si and Al. Nevertheless, they contribute to the polymerization of the melt (see above) and are thus included in the t-parameter. To simplify, we calculate the nbo/t assuming that $t = Si + Al + P + Ti$ and that all Fe is divalent in our experiments, justified by our fO_2 close to iron–wüstite. We then plot the data for element partitioning as a function of nbo/t in the SiO_2-rich melt (nbo/t^F), in which the amount of P and Ti is relatively small, thus reducing the uncertainty in the calculation scheme of nbo/t.

Data from this study and those from Watson (1976b), Visser and Koster van Groos (1979a, b, c) and Freestone and Powell (1983) in the system Fe_2SiO_4–$KAlSi_2O_6$–SiO_2 (with or without P_2O_5, TiO_2, CaO, and MgO) encompass a large pressure (from 0.1 to 1,500 MPa), temperature (1,040°–1,465°C) and compositional range. Only D_{Fe} (FeO^M/FeO^F ratio in wt%) is available for this wide range of conditions, D_{Ca} and D_{Mg} are only from this study and from Watson (1976b). The partition coefficients D_i of the network modifier cations (i = Fe, Mg, Ca) define power law curves when plotted as a function of nbo/t^F (Fig. 5a), the more polymerized the felsic melt is, the less it can accommodate network modifier cations. The fact that the partition coefficient is well correlated with the degree of polymerization (nbo/t)^F suggests that temperature, pressure, or other compositional parameters (e.g., CaO, P_2O_5, TiO_2) have a relatively minor direct effect on the partition coefficients. Of course, these latter parameters influence and determine the shape of the two-melt field, which in turn yields coexisting melt compositions and thus nbo/t of the melts. But any of these parameters appear to be interchangeable and do exert their influence on D_i through the width of the miscibility gap. The most surprising result is the apparent absence of a direct effect of P_2O_5 and TiO_2 on D_{Fe}. First, the chemical potentials of any component in the coexisting melts are equal, so are their activities (all melt components have the same standard state properties, as well as temperature and pressure). For any element, this implies that partition coefficients between the two melts directly reflect a difference of the activity coefficients in the coexisting melts. Secondly, P_2O_5 and TiO_2 enter the silicate melt by forming complexes with network modifier cation, like Fe, suggesting an effect on their activity coefficient. Indeed, Xirouchakis et al. (2001) showed by thermodynamic calculations that the activity coefficient of FeO decreases with increasing TiO_2 through the formation of FeO–TiO_2 compound in the melt. The simplest explanation for this apparent lack of a specific effect of P_2O_5 and TiO_2 on D_is is that the activity coefficients in the SiO_2-poor and SiO_2-rich melts would
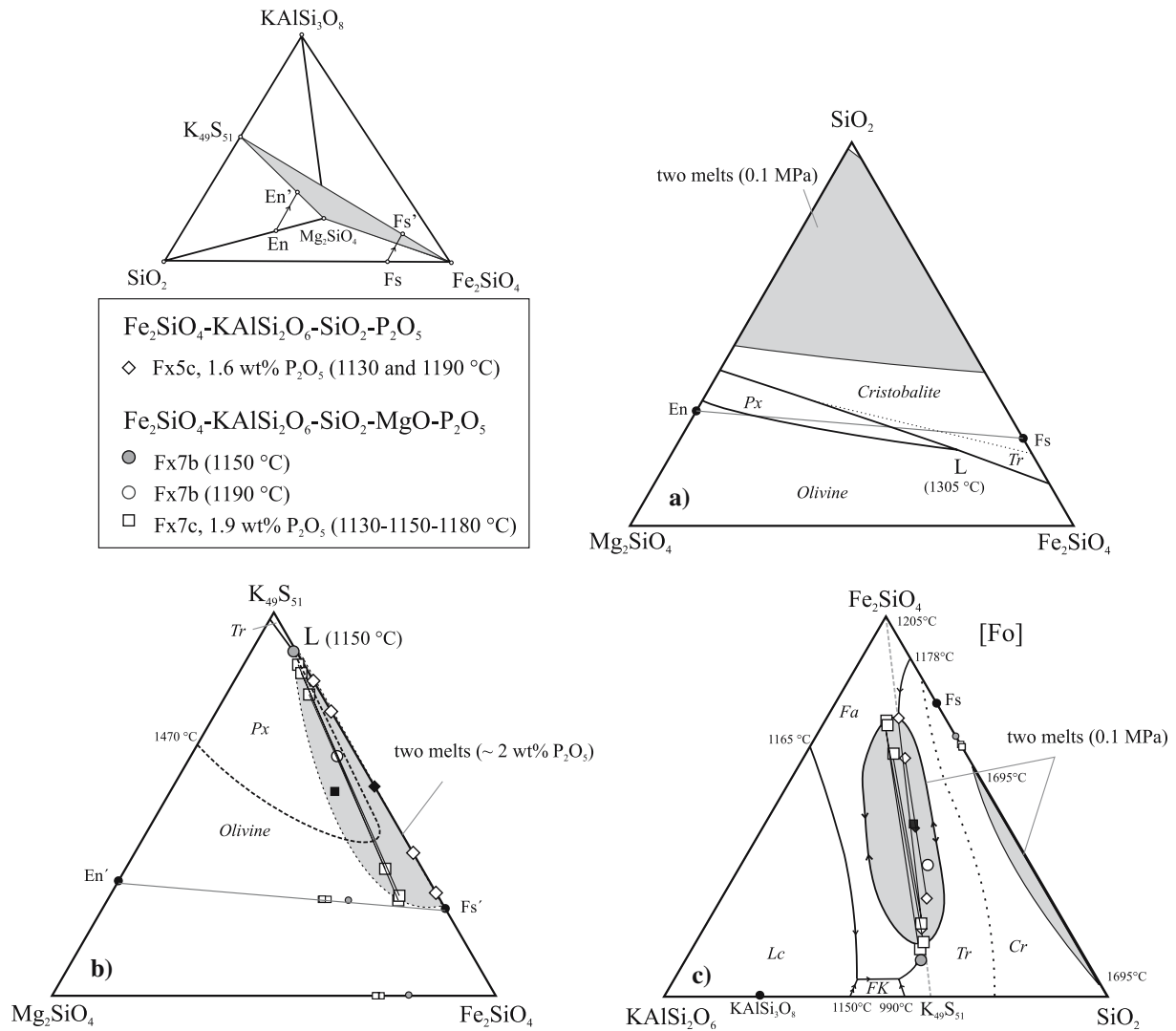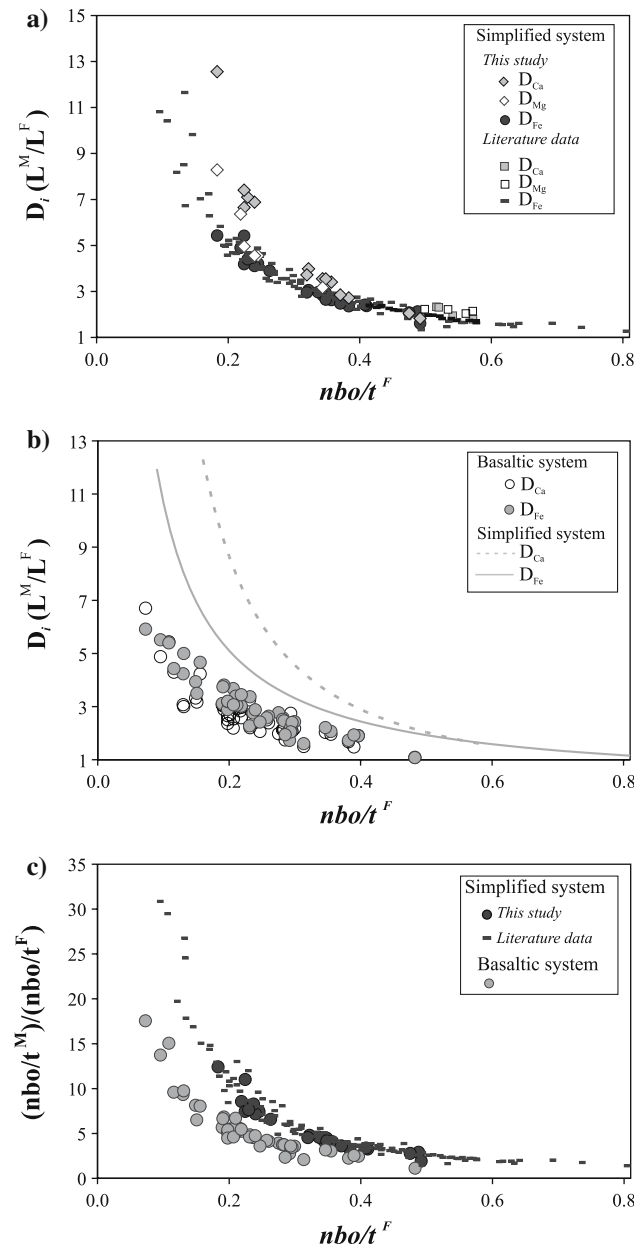
Fig. 4 Melt compositions in the $KAlSi_3O_8$–Mg_2SiO_4–Fe_2SiO_4–SiO_2 tetrahedron projected from TiO_2 and P_2O_5. **a** Mg_2SiO_4–Fe_2SiO_4–SiO_2 plane modified after Bowen and Schairer (1935). The *gray shaded area* corresponds to the immiscibility field at 0.1 MPa. The point L represents the equilibrium between melt, olivine, pyroxene, and trydimite. *Tr* trydimite, *Px* orthopyroxene, *En* enstatite, *Fs* ferrosilite. **b** Mg_2SiO_4–Fe_2SiO_4–$K_{49}S_{51}$ plane.

The various symbols are data from this study. *Black symbols* are the starting materials (*square* Fx7c and Fx7b, *diamond* Fx5c). The *smaller symbols* along the joins En'–Fs' and Mg_2SiO_4–Fe_2SiO_4 are pyroxenes and olivines, the *symbol shape* refers to the melt symbols. **c** Projections form Mg_2SiO_4 [Fo] onto the plane $KAlSi_3O_8$–Fe_2SiO_4–SiO_2

be affected to the same extent by the formation of P and Ti complexes. The activity coefficient ratios would then be only indirectly affected, i.e., through the change in the degree of polymerization produced by P and Ti.

Next, we discuss the experiments on silicate melt immiscibility performed on complex natural compositions at 0.1 MPa (Rutherford et al. 1974; Hess et al. 1975; Dixon and Rutherford 1979; Philpotts and Doyle 1983; Ryerson and Hess 1980; Longhi 1990). These experiments can be described broadly in a basaltic system and those in Fe_2SiO_4–$KAlSi_2O_6$–SiO_2–CaO–

MgO–TiO_2–P_2O_5 as in a simplified system (Watson 1976a, b; Visser and Koster van Groos 1979a, b, c; Freestone and Powell 1983; Schmidt et al. 2006; this study). A similar trend for the dependence of the partition coefficients with $(nbo/t)^F$ is observed in the experiments on both the basaltic and simplified systems but, for a given $(nbo/t)^F$, the partition coefficients of Ca and Fe between the two melts are lower in the basaltic system. The data for D_{Mg} are very scattered (except those from Longhi 1990) and are not plotted in Fig. 5b. This scattering is probably due to the low MgO content in many of the studies in the basaltic system.

a)

b)

c)

Fig. 5 Partition coefficients and nbo/t ratio between coexisting experimental melts (L^M: FeO-rich melt, L^F: SiO_2-rich melt). **a** Variation of the partition coefficient between immiscible liquids for Fe, Mg, and Ca as a function of nbo/t in the SiO_2-rich melt. Literature data for D_{Fe} in the system Fe_2SiO_4–$KAlSi_2O_6$–$SiO_2 \pm P_2O_5 \pm TiO_2 \pm MgO \pm CaO$ are from: Watson (1976b), Visser and Koster van Groos (1979a, b, c) and Freestone and Powell (1983). Data from Schmidt et al. (2006) are included with the data from this study. Power-law equations fitting the data are: $D_{Fe} = 0.92$ (nbo/t^F)$^{-1.06}$, $R^2 = 0.96$; $D_{Mg} = 1.13$ (nbo/t^F)$^{-1.02}$, $R^2 = 0.96$; $D_{Ca} = 0.68$ (nbo/t^F)$^{-1.58}$, $R^2 = 0.96$. **b** Variation of the melt–melt partition coefficients (D_{Fe} and D_{Ca}) in the basaltic system (tholeiitic and lunar basalts). Data from Rutherford et al. (1974), Hess et al. (1975), Dixon and Rutherford (1979), Ryerson and Hess (1980), Philpotts and Doyle (1983) and Longhi (1990). The *two lines* correspond to the power-law curves for D_{Fe} and D_{Ca} in the simplified system (Fig. 5a). **c** Evolution of the width of the two-melt field, expressed by the ratio between nbo/t in the SiO_2-poor and SiO_2-rich melts: [(nbo/t)^M/(nbo/t)^F] against nbo/t in the SiO_2-rich melt

(high-Ti mare basalts), and Al_2O_3 between 8 and 20 wt%. As for the simplified system, the trends of D_i as a function of (nbo/t)^F are valid for a large interval of composition. The main effect of varying the composition is to change the structures of the coexisting melts. As for the simplified system, it is the difference in the degree of polymerization between the two melts which controls element partitioning. Secondly, while the majority of liquid immiscibility experiments in the basaltic system are performed at low fO_2 (near iron–wüstite) some of them are performed between the MW and NNO buffers (mainly at QFM: Dixon and Rutherford 1979; Philpotts and Doyle 1983). In the data set, there are seven experiments at relatively oxidizing conditions, but in D_i versus (nbo/t)^F space, their resulting D_i's cannot be distinguished from those obtained in experiments at low fO_2. Apparently, neglecting the Fe^{3+} in the calculation of nbo/t has only a minor effect.

The difference of D_{Ca} at a given (nbo/t)^F between the two experimental systems could be explained by structural changes, while it is a network modifier in our experiments (Al is completely charge balanced by K in the SiO_2-rich melts), it also enters the tetrahedral Al–Si network as charge compensating cations in immiscibility experiments performed in the basaltic system. This allows a larger amount of Ca in the felsic melt. However, there is no indication for a charge balancing role of Mg or Fe in these melts (the sum of alkalis and Ca is large enough to charge balance the Si^{4+}–Al^{3+} substitution in the tetrahedra), the lowering of the D_is for a given nbo/t^F needs another explanation. Both the experiments in the simplified and basaltic systems result in a correlation between the width of the
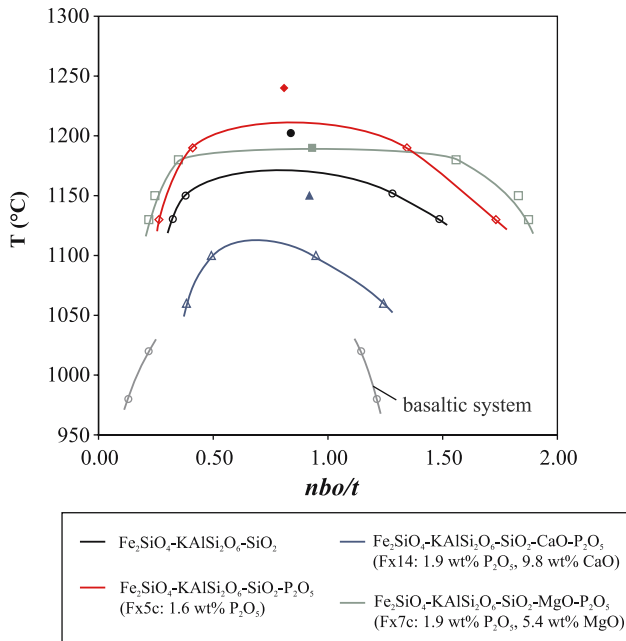
When plotted altogether, data for D_{Ca}, D_{Mg}, and D_{Fe} overlap each other. Actually, the data on basaltic system do not yield a systematic for the relative values between the D_i except for the experiments of Longhi (1990) where the relations $D_{Ca} < D_{Fe} < D_{Mg}$ hold for any given (nbo/t)^F.

To understand the reasons for the difference between the two data sets (simplified vs. basaltic systems), several arguments need to be considered. First, starting materials used in the basaltic system encompass a wide compositional array: with or without P_2O_5, alkali-poor lunar basalts, or relatively Na_2O-rich tholeiitic basalts. TiO_2 varies between 1 and 13 wt%

Fig. 6 Width of the immiscibility gap expressed by nbo/t plotted against temperature. Data for the system Fe_2SiO_4–$KAlSi_2O_6$–SiO_2 are from Visser and Koster van Groos (1979a) and for the basaltic system from Ryerson and Hess (1980)

immiscibility gap [expressed by $(nbo/t)^M/(nbo/t)^F$] and the nbo/t^F (Fig. 5c). However, for a given nbo/t^F, the two-melt field is narrower in the basaltic system. As discussed above, melt polymerization exerts a strong influence on activity coefficients and partition coefficients. A smaller difference in the degree of polymerization of coexisting melts (i.e., a nbo/t ratio closer to unity) should thus cause a proportionally smaller difference in activity coefficients and partition coefficients at a given $(nbo/t)^F$. Differences in element partitioning between the basaltic and simplified systems thus revert
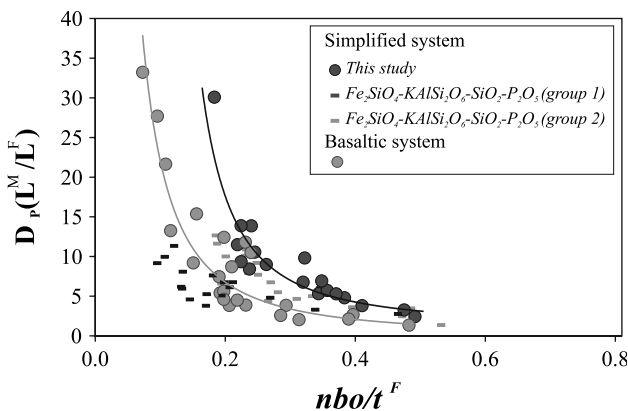

Fig. 7 Variation of partition coefficients for P between immiscible liquids as a function of nbo/t^F. See Fig. 5 for references on the basaltic system. Groups 1 and 2 are from Visser and Koster van Groos (1979c)

to differences in the shape of the two-melt field. The correlations of $(nbo/t)^F$ with the $(nbo/t)^M/(nbo/t)^F$ exist because changing compositions (e.g., addition of CaO, MgO, or P_2O_5, but not $CaAl_2Si_2O_8$) produce a more or less symmetrical variation in the shape of the two-melt field (Fig. 6). However, when $CaAl_2Si_2O_8$ becomes an important melt component, the limbs of the immiscibility gap change asymmetrically compared to the more simplified system (Fig. 6). In composition space, the low-SiO_2 limb retracts at a higher rate than the high-SiO_2 limb compared to the simplified system. Qualitatively, all highly polymerized components in the simplified system (SiO_2, $KAlSi_3O_8$) are enriched in the SiO_2-rich melt, while $CaAl_2Si_2O_8$ is also a tectosilicate unit but is enriched in the SiO_2-poor melt.

Ti and P partitioning

The partition coefficients of P and Ti are plotted in Figs. 7 and 8a, respectively. In our experiments, D_P correlates with nbo/t^F and rises from 2.4 at nbo/$t^F \sim 0.5$ to 30 at nbo/$t^F = 0.18$, indicating that the phosphorus complexes can hardly be accommodated in a polymerized silicate network. The data from experiments on natural compositions plot on a similar curve but with a smaller D_P for a given nbo/t^F. This behavior is similar to the partitioning of Fe, Mg, and Ca and the same reason, i.e., a difference of the shape of the two-melt field between the two systems is proposed (see above).

D_P data from Visser and Koster van Groos (1979b, c) form two distinct groups depending on the Al/K ratio in the SiO_2-rich melt. The first group ($0.90 <$ Al/K < 1.15) plots close to our data ($0.87 <$ Al/K < 0.98) while the second group ($1.13 <$ Al/K < 1.36) plots to lower D_P. Visser and Koster van Groos (1979c) observed that the P_2O_5 content in the SiO_2-rich melt increases with the Al/K ratio and that the Al/(K + P) ratios of these melts are often close to one. They proposed a charge balanced substitution Al + P = 2Si in the aluminosilicate framework. This solution mechanism would increase the solubility of P in polymerized melts, lowers D_P without changing the degree of polymerization, and probably occurs only when K (or in more complex systems, alkalis, and earth alkalis) is insufficient for charge balancing Al in the tetrahedra.

Contrary to other elements, the partition coefficients for Ti are not discernable between the simplified and the basaltic systems (Fig. 8a). The dispersion of the data in the basaltic system does not correlate with the large spread of TiO_2 contents nor with any other single component concentration in the different studies. The
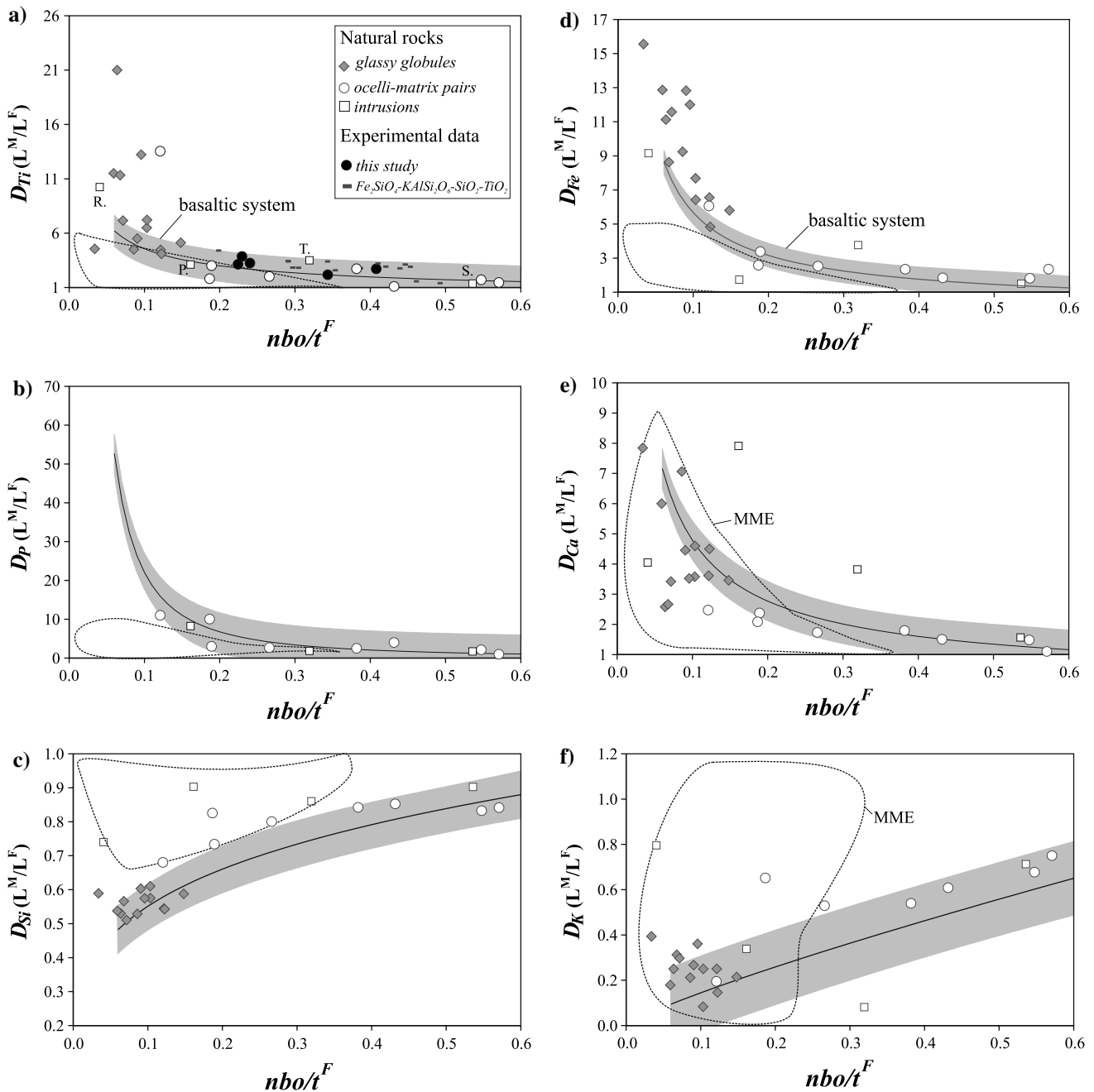
Fig. 8 Comparison of the melt–melt partition coefficients for Ti, P, Si, Fe, Ca, K of the experimental data on the basaltic system (references as Fig. 5b) and natural rocks. Data from the basaltic system are given by the power-law equations fitting the data with 2σ confidence limits as shaded area. D_{Ti} data from this study, Watson (1976b) and Visser and Koster van Groos (1979c). Data for the glassy globules (Philpotts 1982), ocelli-matrix pairs (Philpotts 1976; Foley 1984), intrusions (S.: Shonkin Sag, Kendrick and Edmond 1981; R.: Rosetown, Bender et al. 1982; T.: Triunfo, Ferreira et al. 1994; P.: Putteti, Rajesh 2003). The areas delimited by *dashed lines* correspond to the element ratios between the granitoids and the mafic-microgranular enclaves

(MME) which are not formed through melt immiscibility (see text): Gamble 1979; Reid et al. 1983; Wiebe 1984; Diethelm 1989; Eberz and Nicholls 1990; Zorpi et al. 1991; Bigioggero et al. 1994; Eklund et al. 1994; Nédélec et al. 1995, Bolle 1996; Lowell and Young 1999; Silva 2000; Xu et al. 1999; Roberts et al. 2000. Glassy globules, ocelli, and the Shonkin Sag intrusion plot on the trend defined by the immiscibility experiments in the basaltic system. Coexisting mafic and felsic rocks in the Rosetown, Putteti, and Triunfo intrusions are either not formed through melt immiscibility or the coexisting melts suffered mineral accumulations

increase of D_{Ti} with decreasing nbo/t^F is also smoother than for D_P. When considering experimental data and glassy globules from the mesostasis of volcanic rocks (see below), the sharp increase of D_{Ti} appears near nbo/$t = 0.14$ compared to nbo/$t = 0.22$ for D_P. Titanium can enter the SiO_2-rich melt to a larger extent than phosphorus, probably because it partially enters the Al–Si tetrahedral network, as discussed above.

Immiscibility in natural magmas

Despite the negative effect of MgO, CaO, and pressure on silicate melt immiscibility, our experiments show that this process is viable at mid-crustal pressures when reasonable amounts of P_2O_5 and/or TiO_2 are present. Although our investigated system is still a simplified one, it elucidates the systematics of melt immiscibility and provides the basis for understanding the role of immiscibility in natural silicate melts. Most important, we have quantified the degree of melt polymerization versus element partitioning, similar to what has been deduced from mineral/melt pairs by Kohn and Schofield (1994). This allows assessing natural silicate melts of different compositions at different pressure and temperature: for each pair of coexisting immiscible melts, the polymerization of the SiO_2-rich melt (Fig. 5) directly relates to the partition coefficients of a given element through the power law equations defined in this study. Two limitations of this approach remain. First, when Ca assumes a charge-balancing role for Al in the polymerized network of the SiO_2-rich melt, the relation between the partition coefficients and nbo/t^F is different from the experiments in the simplified system (Fig. 5b). The majority of the natural samples discussed in the following have Al $> (K + Na)$ and tetrahedral Al needs to be charge-balanced by Ca. We will thus mainly use the D_i–nbo/t^F relations obtained from basaltic systems (gray shaded areas in Fig. 8). Secondly, the presence of volatiles (e.g., H_2O, F, S) may interfere with respect to: (1) their effect on the partition coefficients between immiscible melts, which is generally unknown and (2) the calculation scheme for melt polymerization (nbo/t) in which they are not included. Nevertheless, D_is versus nbo/t^F relations hold for a large fO_2 interval (at least between IW-NNO).

Silicate melt immiscibility on Earth has been proposed for both volcanic and plutonic rocks. The first group comprises the glassy globules in the mesostasis of volcanic rocks (Philpotts 1982) and ocelli in lamprophyres (Philpotts 1976; Foley 1984), the second group comprises syenite and granite intrusions (Kendrick and Edmond 1981; Bender et al. 1982; Ferreira et al. 1994; Rajesh 2003). This is not an

exhaustive list but contains well documented examples with well constrained compositions of the proposed coexisting melts.

As a negative test, we have plotted element ratios for mafic microgranular enclaves (MME, Fig. 8) mechanically mingled into a granitic host. These represent unequivocal examples of juxtaposition of co-magmatic melts, which have never been in chemical equilibrium, were not formed through melt immiscibility, and have different mineral compositions, initial isotopic ratios, and usually higher contents of high field strength elements in the felsic, SiO_2-rich melt. They span metaluminous to peraluminous compositions from calc-alkaline, tholeiitic, and shoshonitic series. The element ratios for these mafic enclaves versus their felsic host rocks are clearly distinct for Fe and P (Fig. 8b, d) and are generally lower than for the partition coefficients from immiscible melts for Ti and Ca (Fig. 8a, e), nevertheless, significant superposition occurs for these latter. Al, Si, and alkalis have partition coefficients higher for mafic enclaves versus granitoids than for coexisting immiscible melts, D_{Al} being even greater than one in the former group, but with the exception of Si, some overlap occurs also here.

Immiscibility in volcanic rocks

Glassy globules are mafic and felsic glasses, preserved in the mesostasis of fresh volcanic rocks, typically forming small globules (up to 50 microns) of one within the other. Philpotts (1982) suggested that they formed by melt immiscibility, but Biggar (1979) considered them as formed in a metastable glass state. At least for the tholeiitic rocks, experimental data (Dixon and Rutherford 1979; Philpotts and Doyle 1983) favor Philpotts interpretation. The partition coefficients between the glassy globules from the volcanic rocks (from tholeiitic to alkaline compositions) analyzed by Philpotts (1982) overlap and extend the trends between the partition coefficients and nbo/t^F observed in the experiments from the basaltic system, demonstrating that the relations between partition coefficients and nbo/t^F are valid for a very large range of natural melt compositions.

Ocelli in lamprophyre dykes are another case of proposed immiscibility. They are rounded felsic material (dominated by alkali feldspar and nepheline or quartz) of several millimeter size in a mafic matrix of lamprophyre dykes (Philpotts 1976; Foley 1984). In the Monteregian province (Quebec), the composition of the matrix and the ocelli are close to gabbroic and nepheline syenite–granite intrusions, respectively. Philpotts (1976) suggested that these intrusions could

have formed by immiscibility, in the same way as the ocelli-matrix pairs; the segregation of the coexisting melts almost having completed. However, based on similar data, Bédard ([1994](#)) proposed an alternative model which considers the ocelli as segregations originating from residual interstitial melt fractions. The partition coefficients of major elements between ocelli and matrix plot on, or close to the experimental trends (Fig. [8](#)), favoring the immiscibility model. As a corollary, the presence of H_2O (and probably other fluid components) in the lamprophyric magma seems to have had very limited effects on the relations between D_i versus nbo/t^F defined in anhydrous systems.

Immiscibility in plutonic rocks

Melt immiscibility in intrusions was proposed for a large variety of compositions. Bender et al. ([1982](#)) proposed that the Rosetown granodiorite (near the Cortland complex, New York) and neighboring iron-rich diorites are immiscible melts. The Putteti (India) and the Triunfo (Brazil) syenites contain swarms of pyroxenitic lenses and globules (from few millimeter to several centimeter) considered as an immiscible mafic melt coexisting with a syenitic melt (Ferreira et al. [1994](#); Rajesh [2003](#)). Finally, the Shonkin Sag and Square Butte laccoliths (Montana; Kendrick and Edmond [1981](#)) display textures at centimeter to meter scale suggesting immiscibility between felsic and mafic syenites (shonkinites).

For Ti and P, the intrusions plot on the trend defined by the experiments on the basaltic system and by the glassy globules in the volcanic rocks. However, their partitioning for other elements is more scattered (Fig. [8](#)). We will first discuss the Rosetown and Shonkin Sag plutons and then the Triunfo and Putteti plutons.

The Shonkin Sag laccolith data plot close to the immiscibility trends. However, for the Rosetown intrusion, D_{Fe} and D_{Ca} plot close to the immiscibility trends but the partition coefficients between the granodiorite and diorite for Si, Al, and alkalis plot above these trends (Fig. [8](#)). The difference is particularly pronounced for Al, with $D_{Al} = 0.97$ for the intrusion while this value is 0.4 for experimental immiscible melts in the basaltic system at similar nbo/t^F. The absence of clear enrichment of Al in the SiO_2-rich melt was explained by Bender et al. ([1982](#)) as evidence of accumulated plagioclase in the diorite. The higher D_K could be explained in the same way by accumulation of biotite in the diorite. The occurrence of minerals before the onset of immiscibility is a likely

feature in crystallizing magmas and their accumulation during melt separation certainly plagues any discussion about immiscibility in plutonic rocks.

Almost none of the partition coefficients between the syenites and pyroxenites (Putteti and Triunfo intrusions) plot on the trends defined by the experiments on immiscibility. Actually, in some Harker diagrams (e.g., Al_2O_3, CaO, or K_2O vs. SiO_2), the tie-lines between syenites and pyroxenites are far steeper than for experimental immiscible melts (in simplified and basaltic systems) and the syenites point toward alkali feldspar while the pyroxenites point toward pyroxene. Thus, for these intrusions, rock compositions do not represent coexisting melts. If immiscibility occurred, these melts were modified through accumulation of minerals, i.e., pyroxene and alkali-feldspar for the mafic SiO_2-poor and the felsic SiO_2-rich melts, respectively.

Conclusions

The low-temperature immiscibility field in the system Fe_2SiO_4–$KAlSi_3O_8$–SiO_2 is drastically suppressed by CaO and MgO. However, the addition of small amounts of P_2O_5 or TiO_2 (~ 2 wt%) together with CaO and MgO produce immiscibility at mid-crustal pressures (at least 400 MPa) over a wide temperature interval (1,050° and 1,190°C). Melt–melt partition coefficients for major elements in the system Fe_2SiO_4–$KAlSi_3O_8$–SiO_2–CaO–MgO–TiO_2–P_2O_5, and Fe_2SiO_4–$KAlSi_3O_8$–SiO_2–TiO_2–P_2O_5 depend mainly on the difference between the degree of polymerization (estimated with nbo/t) of the two coexisting melts. Pressure, temperature, and composition can be understood as having an indirect effect on partitioning by determining the width of the two-melt field. The same observation is valid for melt immiscibility in basaltic compositions (tholeiitic and lunar basalts). Natural glassy globules from the mesostasis of tholeiitic and alkaline volcanic rocks (Philpotts [1982](#)), as well as ocelli in lamprophyres from the Monteregian province (Philpotts [1976](#)) plot on, and even extend the trend defined by the experimental immiscible melts in the basaltic system, suggesting that these are formed by melt immiscibility. Our analyses for the Shonkin Sag intrusion suggest that melt immiscibility could be a large scale differentiation process. However, other melt pairs proposed from intrusions (Triunfo, Putteti, Rosetown) are not coexisting melt compositions.

E.B. Watson and an anonymous reviewer improved the manuscript.

References

Bédard JH (1994) Mesozoic east North American alkaline magmatism: Part 1. Evolution of Monteregian lamprophyres, Québec, Canada. Geochim Cosmochim Acta 58:95–112

Bender JF, Hanson GN, Bence AE (1982) The Cortland complex: evidence for large-scale liquid immiscibility involving granodiorite and diorite magmas. Earth Planet Sci Lett 58:330–344

Biggar GM (1970) Molybdenum as a container for melts containing iron oxide. Am Ceram Soc Bull 49:286–288

Biggar GM (1979) Immiscibility in tholeiites. Mineral Mag 43:543–544

Bigioggero B, Colombo A, Del Moro A, Gregnanin A, Macera P, Tunesi A (1994) The Oligocene Valle del Cervo pluton: an example of shoshonitic magmatism in the western Italian Alps. Mem Sci Geol 46:409–421

Bolle O (1996) L'Apophyse du massif stratiforme de Bjerkreim–Sokndal (Rogaland, Norvège): une intrusion composite de la suite charnockitique. In: Demaiffe D (ed) Petrology and geochemistry of magmatic suites of rocks in the continental and oceanic crusts. A volume dedicated to Professer Jean Michot. Université Libre de Bruxelles. Royal Museum of Central Africa (Tervuren), p 129–144

Bowen NL, Schairer JF (1935) The system MgO-FeO-SiO$_2$. Am J Sci 29:151–217

Diethelm K (1989) Petrographische und geochemische Untersuchungen an basischen Gesteinen der Bergeller Intrusion. Ph.D. Thesis, ETH-Zürich, Switzerland

Dixon S, Rutherford MJ (1979) Plagiogranites as late-stage immiscible liquids in ophiolite and mid-ocean ridge suites: an experimental study. Earth Planet Sci Lett 45:45–60

Eberz GW, Nicholls IA (1990) Chemical modification of enclave magma by post-emplacement crystal fractionation, diffusion and metasomatism. Contrib Mineral Petrol 104:47–55

Eklund O, Fröjdö S, Lindberg B (1994) Magma mixing, the petrogenetic link between anorthositic suites and rapakivi granite, Åland, SW Finland. Mineral Petrol 50:3–19

Farges F, Brown GE (1997) Coordination chemistry of titanium (IV) in silicate glasses and melts: IV. XANES studies of synthetic and natural volcanic glasses and tektites at ambiant temperature and pressure. Geochim Cosmochim Acta 61:1863–1870

Ferreira VP, Sial AN, Whitney JA (1994) Large-scale silicate liquid immiscibility: a possible example from northeastern Brazil. Lithos 33:285–302

Foley SF (1984) Liquid immiscibility and melt segregation in alkaline lamprophyres from Labrador. Lithos 17:127–137

Freestone IC (1978) Liquid immiscibility in alkali-rich magmas. Chem Geol 23:115–123

Freestone IC, Powell R (1983) The low temperature field of liquid immiscibility in the system K$_2$O-Al$_2$O$_3$-FeO-SiO$_2$ with special reference to the join fayalite-leucite-silica. Contrib Mineral Petrol 82:291–299

Gamble JA (1979) Some relationships between coexisting granitic and basaltic magmas and the genesis of hybrid rocks in the tertiary central complex of slieve Gullion, Northeast Ireland. J Volcanic Geotherm Res 5:297–316

Hess PC (1977) Structure of silicate melts. Can Mineral 15:162–178

Hess PC (1991) The role of high field strength cations in silicate melts. In: Perchuk LL, Kushiro I (eds) Physical chemistry of magmas, vol 9. Springer, Berlin Heidelberg New York, p 152–191

Hess PC, Rutherford MJ, Guillmette RN, Ryerson FJ, Tuchfeld HA (1975) Residual products of fractional crystallization of lunar magmas: an experimental study. Proceedings of the Lunar Planet Science Conference 6th, vol 1, pp 895–909

Hoover JD, Irvine TN (1978) Liquidus relations and Mg-Fe partitioning on part of the system Mg$_2$SiO$_4$-Fe$_2$SiO$_4$-CaMgSi$_2$O$_6$-CaFeSi$_2$O$_6$-KAlSi$_3$O$_8$-SiO$_2$. Carnegie Inst Washington Year B 77:774–784

Jakobsen JK, Veksler IV, Tegner C, Brooks CK (2005) Immiscible iron- and silica-rich melts in basalts petrogenesis documented in the Skaergaard intrusion. Geology 33:885–888

Kendrick GC, Edmond CL (1981) Magma immiscibility in the Shonkin Sag and Square Butte laccoliths. Geology 9:615–619

Kohn SC, Schofield PF (1994) The importance of melt composition in controlling trace-element behaviour: an experimental study of Mn and Zn partitioning between forsterite and silicate melts. Chem Geol 117:73–87

Kushiro I (1975) On the nature of silicate melt and its significance in magma genesis: regularities in the shift of the liquidus boundaries involving olivine, pyroxene, and silica minerals. Am J Sci 275:411–431

Longhi J (1990) Silicate liquid immiscibility in isothermal crystallization experiments. Proceedings of the Lunar Planet Science Conference 20th, pp 13–24

Lowell GR, Young GJ (1999) Interaction between coeval mafic and felsic melts in the St François Terrane of Missouri, USA. Precam Res 95:69–88

Luth WC (1967) Studies in the system KAlSiO$_4$-Mg$_2$SiO$_4$-SiO$_2$-H$_2$O: pt.1, inferred phase relations and petrologic applications. J Petrol 8:372–416

McBirney AR (1975) Differentiation of the Skaergaard intrusion. Nature 253:691–694

Mysen BO (1983) The structure of silicate melts. Ann Rev Earth and Planet Sci 11:75–97

Mysen BO (1990) Relations between silicate melt structure and petrologic process. Earth Sci Rev 27:281–365

Mysen BO (2004) Element partitioning between minerals and melt, melt composition, and melt structure. Chem Geol 213:1–16

Mysen BO, Ryerson FJ, Virgo D (1980) The influence of TiO$_2$ on the structure and derivative properties of silicate melts. Am Mineral 65:1150–1165

Naslund HR (1983) The effect of oxygen fugacity on liquid immiscibility in iron-bearing silicate melts. Am J Sci 283:1034–1059

Nédélec A, Stephens WE, Fallick AE (1995) The panafrican stratoid granites of Madagascar in a post-collisional extensional setting. J Petrol 36:1367–1391

Philpotts AR (1976) Silicate liquid immiscibility: its probable extent and petrogenetic significance. Am J Sci 276:1147–1177

Philpotts AR (1978) Textural evidence for liquid immiscibility in tholeiites. Mineral Mag 42:417–425

Philpotts AR (1981) A model for the generation of massif-type anorthosites. Can Mineral 19:233–253

Philpotts AR (1982) Compositions of immiscible liquids in volcanic rocks. Contrib Mineral Petrol 80:201–218

Philpotts AR, Doyle CD (1983) Effect of magma oxidation state on the extent of silicate liquid immiscibility in a tholeiitic basalt. Am J Sci 283:967–986

Rajesh HM (2003) Outcrop-scale silicate liquid immiscibility from an alkali syenite (A-type granitoid)-pyroxenite association near Puttetti, Trivandrum Block, South India. Contrib Mineral Petrol 145:612–627

Reid JB, Owen CE, Fates DG (1983) Magma mixing in granitic rocks of the central Sierra Nevada, California. Earth Planet Sci Lett 66:243–261

Roberts MP, Pin C, Clemens JD, Paquette J-L (2000) Petrogenesis of mafic and felsic plutonic rock associations: the calc-alkaline Quérigut complex, French Pyrenees. J Petrol 41:809–844

Roedder EW (1951) Low temperature liquid immiscibility field in the system K_2O-FeO-Al_2O_3-SiO_2. Am Mineral 36:282–286

Roedder EW (1978) Silicate liquid immiscibility in magmas and in the system K_2O-FeO-Al_2O_3-SiO_2: an example of serendipity. Geochim Cosmochim Acta 42:1597–1617

Roedder EW, Weiblen PW (1971) Petrology of silicate melt inclusions, Apollo 11 and 12, and terrestrial equivalents. Proceedings of the Lunar Science Conference 2nd, pp 507–528

Rutherford MJ, Hess PC, Daniel GH (1974) Experimental liquid line of descent and liquid immiscibility for basalt 70017. Proceedings of the Lunar Science Conference 5th, vol 1, pp 569–583

Ryerson FJ (1985) Oxide solution mechanisms in silicate melts: systematic variations in the activity coefficient of SiO_2. Geochim Cosmochim Acta 49:637–649

Ryerson FJ, Hess PC (1978) Implications of liquid-liquid distribution coefficients to mineral-liquid partitioning. Geochim Cosmochim Acta 42:921–932

Ryerson FJ, Hess PC (1980) The role of P_2O_5 in silicate melt. Geochim Cosmochim Acta 44:611–624

Schmidt MW, Connolly JAD, Günther D, Bogaerts M (2006) Element partitioning—the role of melt structure and composition. Science (in press)

Silva MMVG (2000) Geochemistry of enclaves and host granites from the Nelas area, central Portugal. Lithos 50:153–170

Villiger S, Ulmer P, Müntener O, Thomson AB (2004) The liquid line of descent of anhydrous, mantle-derived, tholeiitic liquids by fractional and equilibrium crystallization—an experimental study at 1.0 GPa. J Petrol 45:2369–2388

Visser W, Koster van Groos AF (1979a) Phase relations in the system K_2O-FeO-Al_2O_3-SiO_2 at 1 atmosphere with special emphasis on low temperature liquid immiscibility. Am J Sci 279:70–91

Visser W, Koster van Groos AF (1979b) Effect of pressure on liquid immiscibility in the system K_2O-FeO-Al_2O_3-SiO_2-P_2O_5. Am J Sci 279:1160–1175

Visser W, Koster van Groos AF (1979c) Effect of P_2O_5 and TiO_2 on liquid-liquid equilibria in the system K_2O-FeO-Al_2O_3-SiO_2. Am J Sci 279:970–988

Walker D, Longhi J, Hays JF (1972) Experimental petrology and the origin of Fra Mauro rocks and soil. Proceedings of the Lunar Science Conference 3rd, pp 797–817

Watson EB (1976a) Two-liquid partition coefficients: experimental data and geochemical implications. Contrib Mineral Petrol 56:119–134

Watson EB (1976b) Experimental studies bearing on the nature of silicate melts and their role in trace element geochemistry. Ph.D. Thesis, Massachusetts Institute of Technology, Cambridge, USA

Wiebe RA (1984) Commingling of magmas in the Bjerkrem-Sogndal lopolith (southwest Norway): evidence for the compositions of residual liquids. Lithos 17:171–188

Xirouchakis D, Hirschmann MM, Simpson JA (2001) The effect of titanium on the silica content and on mineral-liquid partitioning of mantle-equilibrated melts. Geochim Cosmochim Acta 65:2201–2217

Xu X, Dong C, Li W, Zhou X (1999) Late Mesozoic intrusive complexes in the coastal area of Fujian, SE China: the significance of the gabbro-diorite-granite association. Lithos 46:299–3159

Zorpi MJ, Coulon C, Orsini JB (1991) Hybridization between felsic and mafic magmas in calc-alkaline granitoids—a case study in northern Sardinia, Italy. Chem Geol 92:45–86